Accepted by Computer Methods in Applied Mechanics and Engineering, 14 Jan 2019

Modeling continuous grain crushing in granular media: a hybrid peridynamics and physics engine approach

Fan Zhu[1] and Jidong Zhao[*1]

[1]Department of Civil and Environmental Engineering,
The Hong Kong University of Science and Technology, Hong Kong SAR, China

*Corresponding author: jzhao@ust.hk

Abstract

Numerical modeling of crushable granular materials is a challenging but important topic across many disciplines of science and engineering. Commonly adopted modeling techniques, such as those based on discrete element method, often over-simplify the complex physical processes of particle breakage and remain a far cry from being adequately rigorous and efficient. In this paper we propose a novel, hybrid computational framework combining peridynamics with a physics engine to simulate crushable granular materials under mechanical loadings. Within such framework, the breakage of individual particles is analyzed and simulated by peridynamics, whilst the rigid body motion of particles and inter-particle interactions are modeled by the physics engine based on a non-smooth contact dynamics approach. The hybrid framework enables rigorous modeling of particle breakage and allows reasonable simulation of irregular particle shapes during the continuous breakage process, overcoming a glorious drawback/challenge faced by many existing methods. We further demonstrate the predictive capability of the proposed method by a simulation of one-dimensional compression on crushable sand, where Weibull statistical distribution on the particle strength is implemented. The simulation results exhibit reasonable agreement with experimental observations with respect to normal compression line, particle size distribution, fractal dimension, as well as particle morphology. The presented work provides a rigorous and efficient way to study the complex process of particle breakage in granular media, and offers future opportunities to examine micro-structural behaviours of crushable granular materials.

Keywords: peridynamics; physics engine; contact dynamics; continuous particle breakage; granular materials

Accepted Manuscript

1. Introduction

Particle breakage signifies a fundamental physical process associated with important industrial handling of granular materials and underpins many macroscopic properties of granular materials such as strength, dilatancy, and permeability [1-3]. Numerical modeling of particle breakage in granular materials holds high practical significance in a wide range of fields including geotechnical engineering, chemical engineering, mining and pharmaceutical industries. Yet the modeling techniques remain far from being rigorous and efficient due to the complex nature of breaking processes. Challenges arise from both the particle level and the representative volume element (RVE) level, where initiation and growth of cracks inside a single grain as well as continuous evolution of particle size and shape in an assembly need to be properly modeled. A desirable numerical approach should enable discrete simulation of a granulate system containing particles with various sizes and shapes which evolve continuously through the loading process. It should allow rigorous modeling of fracturing process of individual particles, while maintaining a practically reasonable computational efficiency. The existing development in particle breakage modeling remains far from being satisfactory.

The research community has long favoured discrete element method (DEM) [4] for the study of granular materials. Breakage of particles has been handled with many simplifications under the framework of DEM. Prevailing approaches include clumped sphere approach [5-8] in which each crushable particle is modeled by multiple elementary spheres/disks bonded together, and particle replacing approach [9-14] where a particle is replaced by several child particles when a pre-set crushing condition is met. Using clumped spheres is computationally expensive and the total number of particles that can be practically simulated is often limited. It is also debatable whether a fracture problem can be reliably simulated by DEM in view of its discrete modeling nature. The particle replacing approach offers better computational efficiency but many assumptions have to be made with respect to the particle crushing conditions and the composition of child particles, which are frequently arbitrary and overly simplified. Importantly, if spheres are used to model the child particles, one tends to neglect particle shape - an important attribute of particles which influences not only the macroscopic material behaviours but also subsequent crushing of an assembly [15]. Recent advances in DEM have witnessed the use of polyhedral particles [16-20] intending for more realistic particle shape modeling. The breakage of particles is handled either by splitting a particle into several smaller polyhedrons [17], or by employing breakable cohesive bonds between pre-defined progenies [21-23] which is conceptually akin to the clumped sphere approach. An alternative approach to model realistic shape particles refers to the level set DEM [24], yet its application in modeling crushable granular materials has not emerged to the best knowledge of the authors. The DEM based approach is in general computationally demanding and its efficiency worsens quickly especially when particle breakage is considered due to drastic increase in number of particles and increasingly small time step required for numerical stability, which limits the appealingness of such approach.

Particle breakage results in continuous transformation of materials from both bulk responses to discrete properties. As such, a hybrid approach, which simulates the physics of both a discrete granular system and particle fracturing process, appears to be appropriate towards more rigorous modeling of crushable granular materials. Various hybrid modeling schemes have been proposed,

Accepted Manuscript

while much attention has been given to the finite-discrete element method (FDEM) [25-29] where DEM is utilized for modeling granular system and finite element method (FEM) is employed for modeling fracturing of individual particles. The approach is computationally demanding and current development in computing power remains unsatisfactory to give a full play to its advantages. Evidently, analyzing continuous particle breakage in 3D cases for a large granular system is overwhelming with the FDEM approach due to excessive cost on remeshing and detailed calculations of stress field within each particle. Some variant approaches to FDEM have also been proposed. For example, Raisianzadeh et al. [30] have combined DEM with extended finite element method (XFEM) since XFEM is less mesh dependent in predicting crack path. Nonetheless, there remain challenges in applying XFEM in handling 3D domain with complex geometrical and loading conditions. There are also a few other hybrid approaches in addition to the FDEM. Prevailing ones include the combination of discontinuous deformation analysis (DDA) with numerical manifold method (NMM) or FEM [31-32]. These methods were often adopted in modeling 2D rock slope failure where rock fracturing is captured by NMM or FEM and sliding of fractured rock pieces is handled by DDA. There appeared no application of such methods for 3D simulation of crushable granular materials, probably due to excessive computational cost.

In this paper we present a novel hybrid computational framework to combine peridynamics with a contact dynamics (CD) based physics engine for simulation of crushable granular materials. The framework is founded on the concept that peridynamics be utilized for breakage analysis of individual particles whilst CD be utilized for modeling the rigid body motions of particles and contact interactions between particles. Peridynamics [33-34] is a continuum-based mesh free method receiving increasing attention in the realm of fracture analysis over the past decade. It has been utilized for simulating fracture in many elastic brittle materials such as rock [35], glass [36], as well as silica sand particles [37]. Geomaterials with more complex behaviors can also be handled with peridynamics by implementing proper material model [38]. The method is adaptive to complex geometries and loading conditions and is computationally efficient, making it advantageous over traditional fracture analysis methods such as XFEM. Nonetheless, peridynamics alone does not support efficient discrete modeling of a particulate granular system due to high computational cost on contact detection and modeling. To compensate such drawback, a CD approach [39-40], or sometimes referred to as non-smooth contact dynamics or granular contact dynamics, has been employed for modeling the granular system. The CD represents an alternative to the traditional, penalty-based DEM. Many open-source libraries, namely physics engines, have been developed based on the concept of CD. Prevailing ones include Bullet [41], Project Chrono [42], Box2D [43-44], and ODE [45]. Although many physics engines were originally developed for fast simulations for games and animations, there have been increasing applications of them in scientific studies. In present study we have chosen the Bullet physics library for simulation, in view that it has been developed and tested in a variety of simulations of granular materials including densification [46], direct shear [47], and granular flow [48-49] where promising results were obtained. There are two-fold reasons for selecting a physics engine for discrete modeling here. First, it allows seamless integration of irregular particle shapes since the contact force network is solved in physics engine as a complementary problem where only contact locations need to be determined. Different particle shapes do not directly incur difficulties in solving the contact forces. This is advantageous over traditional penalty-based DEM where contact force is calculated based on overlapping of particles which

Accepted Manuscript

leads to complex contact modeling algorithms for irregular shape particles [50-52]. Second, unlike the penalty-based DEM which requires time step to be sufficiently small to maintain numerical stability, the CD approach generally allows larger time step and faster computation [49,53]. Such feature is particularly appealing when simulating crushable granular material for which traditional DEM proves to be too expensive.

Specifically, the presented hybrid computational framework serves three undocumented features on particle crushing modeling. First, it offers a rigorous way to model breakage of individual particles by peridynamics instead of imposing a variety of arbitrary assumptions on breakage conditions and breakage patterns. Continuous particle breakage is readily handled by peridynamics too. Second, particles are modeled using polyhedrons which allows more realistic modeling of particle morphologies during the continuous crushing process. Moreover, the overall computational cost can be maintained in practically acceptable range as both physics engine and peridynamics are efficient for the tasks they are assigned to. Nonetheless, there remain room to further improve its computational efficiency by implementing GPU based parallel computing techniques, which is beyond the scope of current study but points out a viable direction for future development of the presented framework.

In what follows, we first present the theoretical basis and principle for the hybrid peridynamics and physics engine method. We then employ the proposed method to simulate a one-dimensional (1-D) compression of crushable sand as a demonstration. Weibull statistics on particle strength [54-56] has been implemented in the simulation to describe the strength of natural material. Comparison with experimental records is made for the simulation results for validations. Further discussion is made regarding its potential and future development in analyzing crushable granular media.

2. Theory

2.1 Peridynamics

In the present study we employ peridynamics for modeling breakage of single grains. The method utilizes a particle-based approach for modeling continuum material. A material domain is first discretized into peridynamic material points, each representing a certain volume of the continuum body. The material points interact with each other through peridynamic bonds established between a material point and each other point within its family. The family of a material point is defined by *horizon* as illustrated in Fig. 1(a). In the current study, the *ordinary state-based peridynamics* [34] is employed, with an assumption that the modeled particles are isotropic material. The basic equation can be written as:

$$\rho(\boldsymbol{x})\ddot{\boldsymbol{u}}(\boldsymbol{x},t) = \int_{\mathcal{H}_x} [\boldsymbol{T}(\boldsymbol{x},t) < \boldsymbol{x}' - \boldsymbol{x} > - \boldsymbol{T}(\boldsymbol{x}',t) < \boldsymbol{x} - \boldsymbol{x}' >] \, dV_{x'} + \boldsymbol{b}(\boldsymbol{x},t) \tag{1}$$

where $\rho(\boldsymbol{x})$ represents material density at material point $\boldsymbol{x}$, $\boldsymbol{u}(\boldsymbol{x},t)$ represents the displacement of material point $\boldsymbol{x}$ at time t. The force state $\boldsymbol{T}$ quantifies bond force between a material point and a

Accepted Manuscript

neighboring point. $\boldsymbol{\mathcal{H}}_x$ represents the neighborhood set of $\boldsymbol{x}$, $dV_{x'}$ is the volume represented by $\boldsymbol{x}'$, and $\boldsymbol{b}$ denotes a body force density.

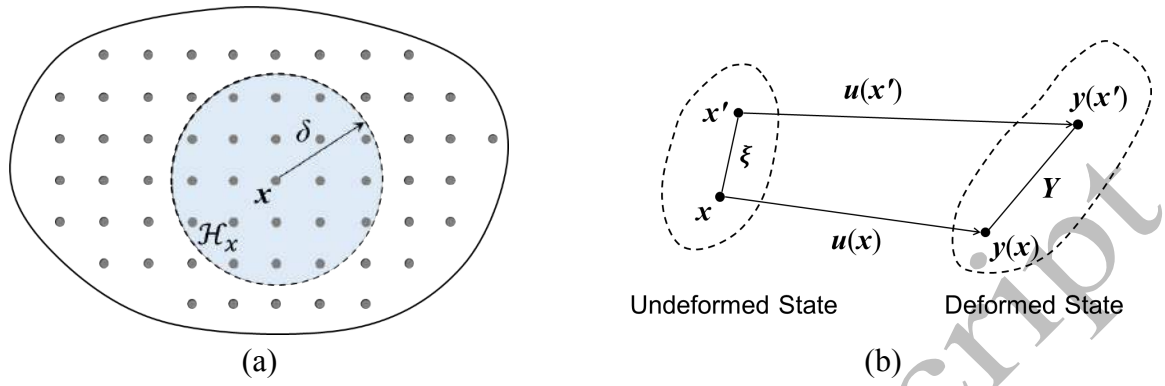

Fig. 1. Illustration of concepts in peridynamics: (a) peridynamic material point $\boldsymbol{x}$ and its family $\boldsymbol{\mathcal{H}}_x$, defined by a horizon $\boldsymbol{\delta}$; (b) bond vector $\boldsymbol{\xi}$, displacement vector $\boldsymbol{u}$, and deformation vector $\boldsymbol{Y}$.

In the present study we adopt a linear peridynamic solid (LPS) material model [34] which is a non-local analogy to the classical linear elastic material model. In LPS model, the force state $\boldsymbol{T}$ is calculated by:

$$\boldsymbol{T} = \left(\frac{3K\vartheta}{m\langle\boldsymbol{x}\rangle}\phi\underline{x} + \frac{15\mu}{m\langle\boldsymbol{x}\rangle}\phi\underline{e}^d\right)\frac{\boldsymbol{Y}}{\|\boldsymbol{Y}\|} \tag{2}$$

where μ and K represent shear and bulk modulus, respectively, ϕ is an influence function taken to be one in this study. $\boldsymbol{Y}$ represents deformation vector between two material points $\boldsymbol{x}$ and $\boldsymbol{x}'$ as illustrated in Fig. 1(b). $\boldsymbol{Y}$ can be calculated by $\boldsymbol{\xi} + \boldsymbol{u}(\boldsymbol{x}', t) - \boldsymbol{u}(\boldsymbol{x}, t)$where $\boldsymbol{\xi}$ represents the bond vector between $\boldsymbol{x}$ and $\boldsymbol{x}'$. $\underline{x}$ is a position scalar state whose value at $\boldsymbol{\xi}$ equals $\|\boldsymbol{\xi}\|$. $m\langle\boldsymbol{x}\rangle$ defines a weighted volume at material point $\boldsymbol{x}$ and ϑ represents dilation. They are defined as:

$$m\langle\boldsymbol{x}\rangle = \int_{\mathcal{H}_x} \phi\|\boldsymbol{\xi}\|^2\, dV_{x'} \tag{3}$$

$$\vartheta\langle\boldsymbol{x}\rangle = \frac{3}{m\langle\boldsymbol{x}\rangle}\int_{\mathcal{H}_x} \phi\|\boldsymbol{\xi}\|\underline{e}\, dV_{x'} \tag{4}$$

where the scalar extension state $\underline{e}$ consists of an isotropic part $\underline{e}^i$ and a deviatoric part $\underline{e}^d$, and can be calculated by $\underline{e} = \underline{e}^i + \underline{e}^d = \|\boldsymbol{Y}\| - \|\boldsymbol{\xi}\|$. The isotropic part is defined by $\underline{e}^i = \vartheta\langle\boldsymbol{x}\rangle\underline{x}/3$ and the deviatoric part can be obtained by subtracting the isotropic part from the scalar extension state.

Fracturing is modeled by allowing the peridynamic bonds to break. Once broken, a bond no longer carries any force and the force originally borne will be redistributed to its neighboring bonds. Such process may lead to successive breakage of bonds and eventually form a fracture surface. Breakage of peridynamic bonds is determined by a critical stretch damage model [57],

Accepted Manuscript

where a bond is considered broken when its strain reaches a critical level, s_c, defined according to Madenci & Oterkus [58] as:

$$s_c = \sqrt{\frac{G_c}{\left(3\mu + \left(\frac{3}{4}\right)^4 \left(K - \frac{5\mu}{3}\right)\right)\delta}} \tag{5}$$

where δ represents the horizon and G_c represents critical energy release rate which is a material constant that can be determined from experiment. For the sand particles modeled in this study, the G_c is taken to be 30 J/m^2 for a base case where a 2 mm diameter particle has a characteristic strength of 45 MPa in consideration of past experimental study [59] and calibration with single particle crushing tests [60]. The horizon is taken to be 3 times of the element size in a cubic pattern discretization following common practice in peridynamic modeling [61-63].

Although literatures have shown that peridynamics can also be used to handle discrete objects by implementing a spring-like contact model between material points [57,64-66], the contact detection and modeling were found to be excessively time consuming which prevents its application in simulating a large number of three-dimensional discrete objects [64]. As such, to handle a granular system with crushable particles, peridynamics alone appears inadequate, and a separate discrete modeling tool is necessary to form an efficient numerical framework.

2.2 Discrete modeling

In the present study we employ the Bullet physics engine, which follows a CD approach, for modeling granular system. Application of physics engine in simulating granular materials is relatively recent. The embedded procedures in physics engine may be categorized into three phases: collision detection, contact resolution and time integration. In the Bullet physics engine, collision detection is performed in two phases, initiated by a broad phase which utilizes axis-aligned bounding box (AABB) algorithm to identify objects that can potentially collide, and followed by a narrow phase which determines the location of contact points and penetration depth if objects overlap. For convex polyhedrons, the Gilbert-Johnson-Keerthi (GJK) algorithm [67] is utilized for collision detection, supplemented by an expanding polytope algorithm (EPA) [68] for computing penetration depth when overlapping occurs. The GJK algorithm computes Minkowski difference of two convex hulls to determine if they collide. It has been recognized as an efficient algorithm for contact detection of convex shapes and prevails in physics engines. For concave polyhedrons (with triangulated surface), collision detection is performed on triangle level, making the computation more expensive than that of convex shapes. Therefore, simplifying a concave shape into convex shape is demanded if the object does not possess high concavity.

In physics engine, contact forces and external forces are modeled by impulses which alter the velocity of objects instantly. Consequently, the velocity of objects is non-smooth and the viscoelastic nature of contact event is not modeled. Such approach is favorable for simulating quasi-static or slow flow process of samples consisting of high stiffness materials [53]. Unlike traditional penalty-based DEM, where a slight overlapping between contacting objects is

Accepted Manuscript

computed and used for solving contact force, the physics engine theoretically does not cause objects to overlap and contact forces are obtained by solving constraint equations. For a pairwise contact case shown in Fig. 2, the constraints can be presented by:

$$v_n = (\boldsymbol{v}_2 - \boldsymbol{v}_1) \cdot \boldsymbol{n} \geq 0 \tag{6a}$$

$$v_t = (\boldsymbol{v}_2 - \boldsymbol{v}_1) \cdot \boldsymbol{t} = 0 \tag{6b}$$

on the normal and tangential directions, respectively. $\boldsymbol{v}_1$ and $\boldsymbol{v}_2$ represent the velocity at contact point on object 1 and 2, respectively. v_n and v_t thus represent the relative normal and tangential velocity of the two objects at the contact point, respectively. The normal constraint presented in Eq. (6a) reinforces that colliding objects will not move further toward each other (which incurs overlapping). The frictional constraint presented in Eq. (6b) tends to eliminate the relative movement of the colliding objects and the magnitude of frictional impulse is bounded by the Coulomb's law of friction.

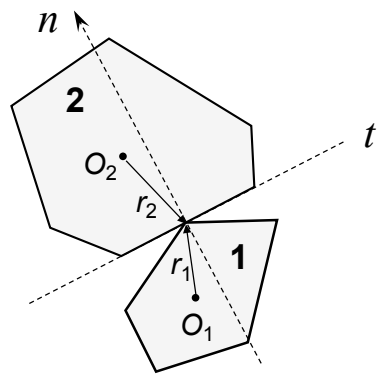

Fig. 2. Two colliding polygonal objects.

Implementation of the constraints stays on velocity and impulse level. At the time of constraints violation, a normal impulse and a tangential impulse as expressed by Eq. (7a) & (7b) will be applied on the colliding objects:

$$p_n = \frac{-(1+e)v_n}{1/m_1 + 1/m_2 + \boldsymbol{I}_1^{-1}[(\boldsymbol{r}_1 \times \boldsymbol{n}) \times \boldsymbol{r}_1 \cdot \boldsymbol{n}] + \boldsymbol{I}_2^{-1}[(\boldsymbol{r}_2 \times \boldsymbol{n}) \times \boldsymbol{r}_2 \cdot \boldsymbol{n}]} \tag{7a}$$

$$p_t = \frac{-v_t}{1/m_1 + 1/m_2 + \boldsymbol{I}_1^{-1}[(\boldsymbol{r}_1 \times \boldsymbol{t}) \times \boldsymbol{r}_1 \cdot \boldsymbol{t}] + \boldsymbol{I}_2^{-1}[(\boldsymbol{r}_2 \times \boldsymbol{t}) \times \boldsymbol{r}_2 \cdot \boldsymbol{t}]} \tag{7b}$$

where e represents restitution whose magnitude equals the ratio of rebounding velocity and impacting velocity. For a sample consisting of closely packed particles, an effective restitution of zero can be expected [40]. m_1, m_2 and $\boldsymbol{I}_1$, $\boldsymbol{I}_2$ represent mass and moment of inertia of the two objects, and $\boldsymbol{r}_1$ and $\boldsymbol{r}_2$ represent vector from centroid to the contact location in the two objects as illustrated in Fig. 2. The normal impulse is a nonnegative value and the frictional impulse is bounded by Coulomb's friction law which can be expressed by $-fp_n \leq p_t \leq fp_n$ where f represents the coefficient of friction. Ideally, objects do not overlap if collision events can be well identified during the simulation. Practically, however, overlapping may occur due to insufficiently small time step. At the moment of particle crushing, the child particles may also experience a slight overlapping initially as a result of simplifications we made to the morphology

Accepted Manuscript

of child particles. A stabilization scheme [69] has been implemented to separate objects that have overlapped by applying a repulsive velocity, v_d, to the overlapping objects:

$$v_d = \beta \frac{\Delta d}{\Delta t} \tag{8}$$

where Δd is penetration depth and β is a penetration correction factor. A large β may quickly pull the overlapping objects apart but introduce apparent kinetic energy and drive the simulation unstable, whereas a too small β may not effectively separate overlapped objects. The factor is taken to be 0.003 for the problem simulated in this paper based on our experience.

For a multi-body constraint system, the contact force network is mathematically considered as a complimentary problem (CP) [39]. The Bullet physics engine uses a Projected Gauss-Seidel (PGS) approach to solve the CP iteratively. In each iteration, the contact impulses at each pairwise contact are calculated based on the constraint conditions shown in Eq. (6a) & (6b) and the pairwise solutions shown in Eq. (7a) & (7b). After sufficient number of iterations, an admissible solution of the contact force network can be obtained. The number of iterations, N_{itr}, largely affects the accuracy of the solution in the PGS solver. Practically, a relative error defined by $\varepsilon = \|f^{k} - f^{k-1}\| / \|f^{k}\|$ may be used to gauge the convergence of results where f^{k} represents the solution vector at k^{th} iteration. Asking for a very low ε would require a large N_{itr} which raises computational cost significantly [40] but deems unnecessary, while over-relaxing the requirement on ε may not provide sufficient accuracy. For a large granular system, the solution may not be unique from a mathematical point of view. Focuses are placed on finding an admissible solution on statistical or macroscopic level rather than the reproducibility of solution at local contact points. In the current study we conservatively adopted N_{itr} = 2000 for the majority of the simulation except at the beginning when the number of particles is small. The relative error in the iterations is generally controlled near or below 2×10^{-4}. The PGS method has provided a practical computational efficiency in current study. Nonetheless, it needs to be mentioned that a variety of other methods exist for solving CP, including direct methods such as the Lemke algorithm [70], and iterative methods such as the conjugate gradient and quadratic programming methods [71]. The PGS method is prevailing in physics engines probably due to its high efficiency in single iteration, ease in implementation, and small memory usage. For a large granular system consisting of particles with variable sizes, nonetheless, the PGS approach may not perform the best and it is worthwhile to explore other methods for better accuracy and efficiency, which may pave a further development to the numerical framework presented in this paper.

Upon solving the contact impulses, the linear and angular velocities of objects are updated by:

$$\boldsymbol{v}_{(t+\Delta t)} = \boldsymbol{v}_t + m^{-1}\left[(\boldsymbol{f}^b + \boldsymbol{f}^{ext})\Delta t + \sum \boldsymbol{p}^c\right] \tag{9a}$$

$$\boldsymbol{\omega}_{(t+\Delta t)} = \boldsymbol{\omega}_t + \boldsymbol{I}^{-1}\left[(\boldsymbol{r}_b \times \boldsymbol{f}^b)\Delta t + (\boldsymbol{r}_{ext} \times \boldsymbol{f}^{ext})\Delta t + \sum (\boldsymbol{r}_i \times \boldsymbol{p}^c)\right] \tag{9b}$$

where $\boldsymbol{f}^{b}$ and $\boldsymbol{f}^{ext}$ represent body force and external force, respectively, $\boldsymbol{r}_b$ and $\boldsymbol{r}_{ext}$ represent the vector from centroid to the point where force acts, and $\boldsymbol{p}^c$ represents contact impulse. The actual implementation of Eq. (9a) & (9b) is performed in a sequential manner in the Bullet physics engine, in other words, the velocities of objects are updated at each iteration. Contact force is not

Accepted Manuscript

directly computed but may be retrieved from the calculated contact impulse. Under quasi-static or slow flow conditions, the contact force may be assumed constant over the time step Δt. Dividing the contact impulse by time step Δt yields the contact force [49]. Time integration is performed following:

$$\boldsymbol{y}_{(t+\Delta t)} = \boldsymbol{y}_t + \boldsymbol{v}_{(t+\Delta t)}\Delta t \tag{10a}$$

$$\boldsymbol{\theta}_{(t+\Delta t)} = \boldsymbol{\theta}_t + \boldsymbol{\omega}_{(t+\Delta t)}\Delta t \tag{10b}$$

where $\boldsymbol{y}$ represents position and $\boldsymbol{\theta}$ represents rotation. The time integration scheme is known as the symplectic Euler scheme which offers good numerical stability [49] and allows the use of large time steps. For scientific simulations of granular material, a time step size on the order of 10^{-4} to 10^{-5} s is often adopted [40], which is several orders larger than the time step size typically used in traditional DEM simulations, offering competitive computational efficiency.

3. Hybrid peridynamics-physics engine approach for continuous grain crushing

3.1 Computational scheme

The proposed framework integrates peridynamic method and physics engine for simulation of crushable granular material. A computational scheme of the framework is shown in Fig 3. The coupling of the two methods may be described by three major procedural stages as discussed below with more technical details provided in the following section.

Stage 1: Select particles for breakage analysis. Apparently, it is neither economical nor necessary to perform breakage analysis for each single particle in an assembly at each time step of the physics engine computation. In this study we check the breakage of particles at prescribed loading steps in the physics engine (e.g., every 0.08MPa vertical pressure interval of the 1D compression problem). Selection of the interval for particle breakage analysis is based on a balanced consideration of both accuracy and computational efficiency. A large interval may save computational cost but underestimate the number of breakage events and adversely affect the accuracy of the simulation. A small interval, on the other hand, can theoretically track the breakage process more realistically, but at higher computational cost. One should select an interval according to the specific need from the simulation and a sensitivity study is advisable. At each time of breakage analysis, a screening process is conducted first to select particles which are most likely to break. A breakage analysis threshold is established based on the maximum contact force on a particle, F_{max}, for the screening process. Adopting such a criterion has good supports from a variety of studies [37,72-73] where it has been suggested to be a reasonable simplified criterion to determine breakage of a particle. For a spherical sand particle of 2.0 mm diameter crushed under uniaxial forces, a F_{max} of approximately 180 N was recorded in both our simulation and previous experiments [60]. The breakage analysis threshold was conservatively set at 80 N, in view that different particle shapes and loading patterns may result in different F_{max} at crushing. For particles with different sizes and strengths, the threshold is adjusted based on the formulations presented in Section 4. The purpose of the screening process is to keep particles that are unlikely to break out of the pool for breakage analysis, which is critical for efficient simulation.

Accepted Manuscript

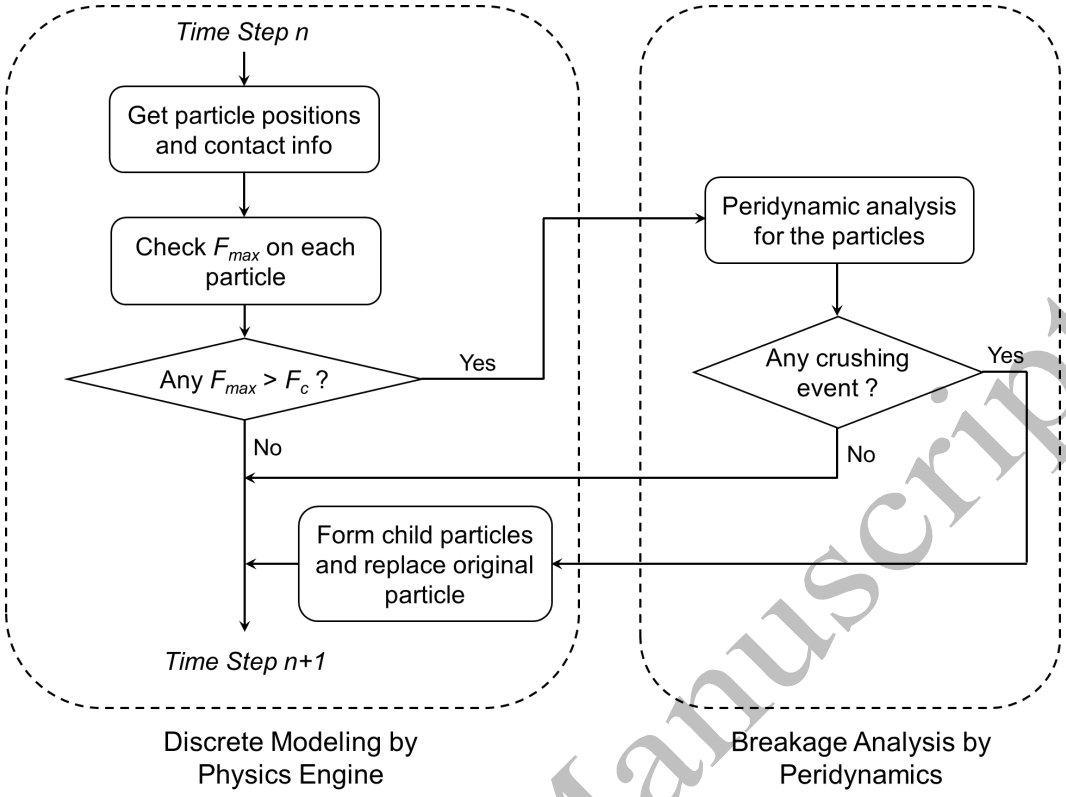

Fig. 3. Computational scheme of the combined peridynamics and physics engine framework.

Stage 2: Initialize and perform peridynamic analyses. A peridynamic analysis is set up for each particle selected for breakage analysis. A particle is discretized into peridynamic material points following a cubic pattern. In the present study, the element size is selected to be approximately $0.062d_e$ where d_e is the equivalent diameter of the particle (i.e., the diameter of a sphere having the same volume to the particle). Such discretization density in general creates 2000 to 2500 material points for each particle after discretization, which offers reasonable results in our simulations. A denser discretization may achieve better accuracy in obtaining fracture surface at the cost of computational efficiency. However, as we do not intend to model local morphology of particles with extremely high resolution, using a denser discretization appears to be unnecessary. A sensitivity study also reveals that denser discretization does not lead to noticeable change in macroscopic results as presented in Section 5. Contact forces are applied at contact locations obtained from the physics engine. Since peridynamics does not allow traction boundary condition, contact force is applied on a volume defined by a contact radius as illustrated in Fig. 4. In the present study the contact radius is taken to be 2 times the element size. Contact force is uniformly distributed among the material points within the assumed contact zone. Application of contact forces follows linear increment with time. The contact zone corresponding to the maximum contact force is fixed to prevent movement or rotation of the particle during peridynamic analysis. No force will be applied to material points within the fixed zone.

Accepted Manuscript

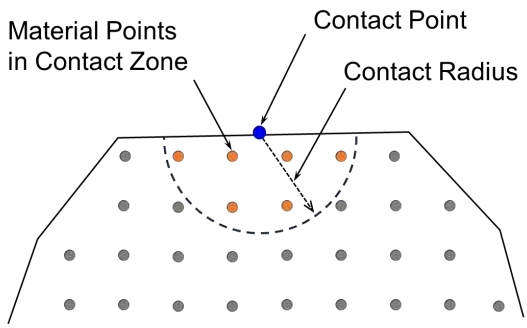

Fig. 4. Illustration of assumed contact zone

In this framework, the peridynamic analyses of individual particles are designed to be independent of each other. A parallel computing scheme is implemented by distributing the work among multiple threads on CPU, which brings remarkable enhancements on computational efficiency. For instance, if 100 particles are selected for breakage analysis simultaneously and the time for analyzing each particle is similar, with a paralleled computing on 4 CPU threads, each thread will be allocated approximately 25 particles for peridynamic analysis and the computing time can theoretically be reduced to about 25% of that without parallel computing. If a more powerful computing facility is available, e.g., with 36 CPU threads, the computing time may be theoretically reduced to about 3% of that without parallel computing.

Stage 3: Build child particles when breakage occurs. Following the peridynamic analysis, a particle may be found either intact or split into several major pieces. In the former case, the particle will be kept in the physics engine. In the latter case, child particles will be built based on peridynamic analysis results and the original particle will be replaced by the child particles in physics engine before advancing the time step. This procedure is further delineated in the following section as it contains several technical procedures.

3.2 Building child particles

At completion of the peridynamic analysis, the status of the particle can be determined by reviewing damage of peridynamic bonds. Here we only consider bonds between immediate neighboring points for efficiency and robustness of the algorithm. For a crushed particle, the broken pieces can be viewed as several clusters of material points which are internally connected by the bonds but isolated with each other. Fig. 5 gives a 2D illustration of such concept (our following simulation is 3D). When the domain is split into two pieces, every point inside either Piece 1 or Piece 2 are connected through bonds, but no connectivity can be found between the two pieces. Therefore, a particle is considered crushed if more than one major cluster of material points can be identified. Breakage of a particle often generates several major broken pieces together with many fine fragments. In this study, a child particle is defined to have no less than 3% of the volume of its parent particle (this threshold is of course adjustable subject to practical need). Consequently, the fine fragments, as represented by isolated material points in peridynamic analysis, are not modeled as child particles to save computational cost. However, to maintain mass and volume conservation, those fragments are not ignored but are “attached” to the nearest major pieces.

Accepted Manuscript

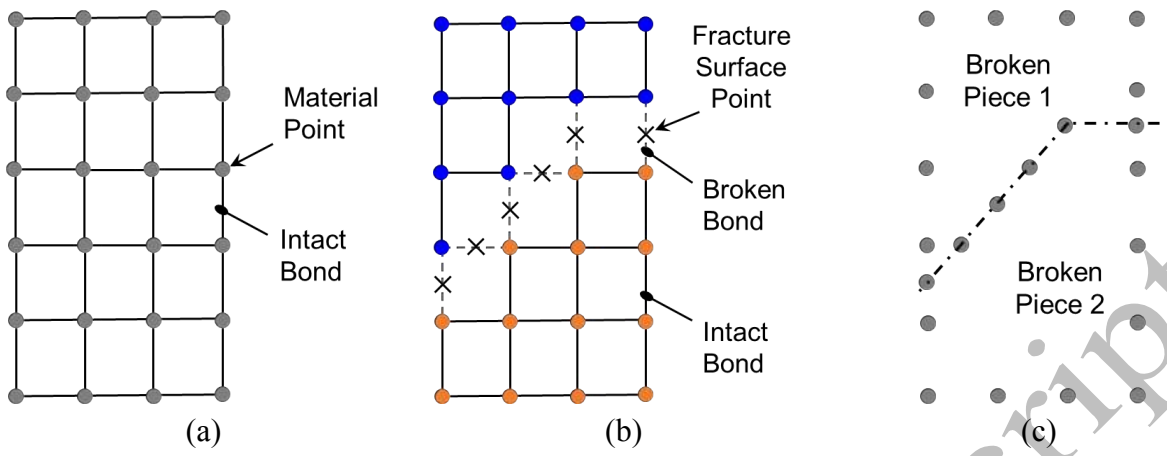

Fig. 5. A 2D illustration of the process of building vertices of child particles based on peridynamic analysis results. (a) original and intact domain; (b) obtain fracture surface points from peridynamic analysis results; (c) define vertices for broken pieces.

Building the morphology of child particles consists of two key steps. The ***first*** step is to build boundary vertices of the child particles as illustrated in Fig. 5. The boundary of a child particle consists of fracture surface points and original domain boundary points. The fracture surface points are created by taking arithmetical average of two points sharing a broken bond. The ***second*** step is to build polyhedron based on the boundary vertices. Here we utilize the concept of 3D alpha shape [74] and employ the Computational Geometry Algorithms Library (CGAL) [75] to perform the task. Alpha shape is a technique commonly used for surface reconstruction from a set of unorganized data points [76]. The process of building a 3D alpha shape from a point set is illustrated in Fig. 6. The point set itself as shown in Fig. 6(a) can be seen as an alpha shape with alpha value of zero. While increasing the alpha value, edges and faces will form and eventually a convex hull is obtained when the alpha value is large enough. The process of building a polyhedron of child particle seeks for a proper stopping criterion, or in other words, a proper alpha value which renders a polyhedron that does not self-intersect, and bears no singular edges and faces. Such requirement can be quantified by requiring the Euler characteristic to be 2, or expressed by $V + F - E = 2$ where V, F, and E represent number of vertices, facets, and edges of the polyhedron, respectively. Fig. 6(c) illustrates a generated child particle using such criterion. The generated polyhedron may be either convex or concave. Nonetheless, considering the high computational cost associated with modeling concave shapes, any polyhedron having equivalent diameter less than 0.7 mm or convexity not less than 0.85 are further simplified to its convex hull for discrete modeling in this study. The convexity is defined by the ratio of the volume of a polyhedron to the volume of its corresponding convex hull. Such simplification ignores local morphology features of the particles but offers appreciable savings on computational cost. The overall shape characteristic of particles, such as the elongation, flatness and aspect ratio, are not expected to be apparently affected by such simplification. A drawback of simplifying particles into convex shapes is that the total volume of child particles will be slightly larger than the volume of the parent particle. To ensure mass and volume conservation, the generated child particles are shrunken slightly until the total volume of child particles equals the volume of the parent particle.

Accepted Manuscript

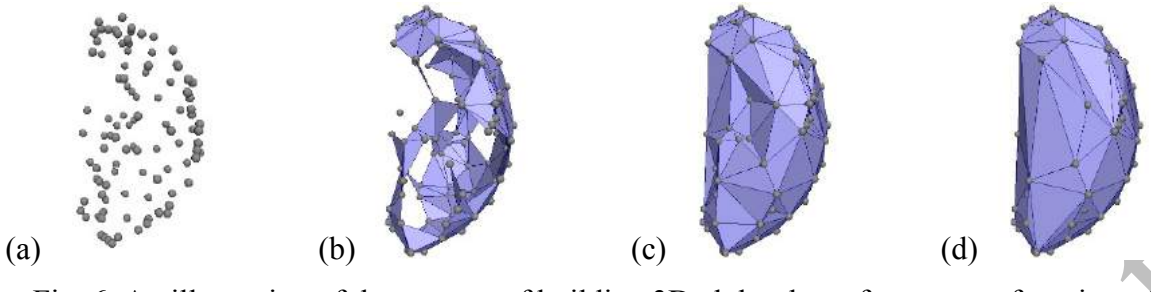

Fig. 6. An illustration of the process of building 3D alpha shape from a set of vertices. (a) vertices defining a particle; (b) generated shape with a small alpha value; (c) a non-self-intersecting polyhedron with concave features obtained with a sufficient alpha value; (d) a convex hull polyhedron obtained with a large alpha value.

The child particles are then created in physics engine, occupying the space originally occupied by their parent particle, with the original particle removed. The child particles may experience slight overlapping immediately after they are created, which will be resolved quickly through the overlapping correction procedure presented in Eq. (8). A complete process of initialization of peridynamic analysis and constructing child particles is illustrated in Fig. 7.

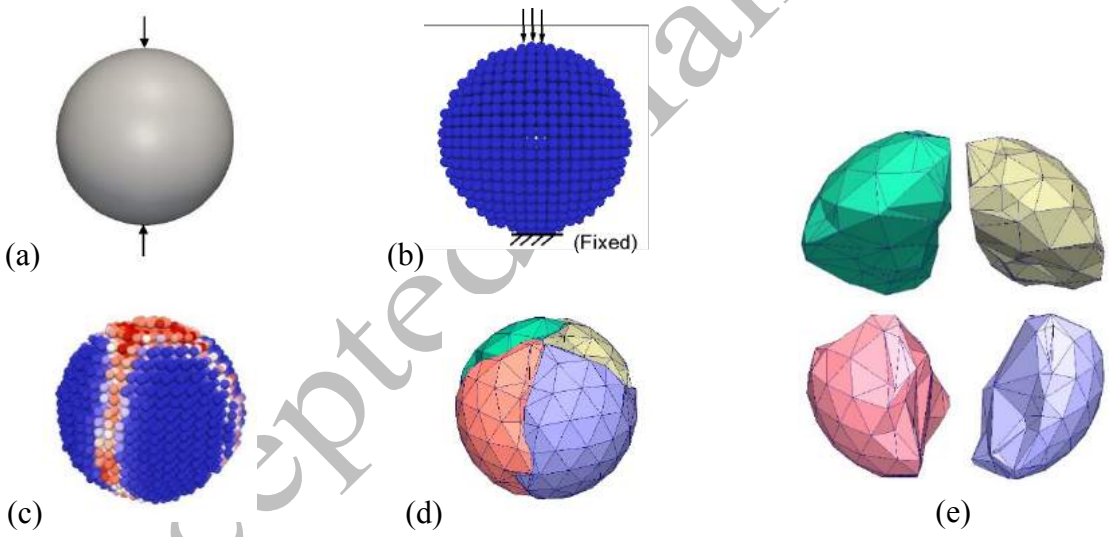

Fig. 7. Illustration of modeling process of a particle undergone crushing: (a) a particle subjected to contact forces; (b) discretized particle for peridynamic analysis; (c) peridynamic analysis result indicating crushing of the particle; (d) modeled child particles in physics engine; and (e) a split view of the child particles.

4. Implementation of statistical particle strength

4.1 Weibull distribution of particle strength

For natural sand, a good number of studies have shown that particle strengths follow Weibull statistical distribution [2,77-79] which defines survival probability of particles by an exponential function:

Accepted manuscript

$$P_s = exp\left[-\left(\frac{d}{d_0}\right)^3\left(\frac{\sigma}{\sigma_0}\right)^{\psi}\right] \tag{11}$$

where P_s represents survival probability of a particle with a size d and a characteristic strength σ. Under typical experiment settings, the characteristic strength of a particle is calculated by dividing the applied uniaxial force by the square of particle size [79]. In the current study, the particle size refers to the equivalent diameter of a particle. σ_0 represents characteristic strength corresponding to 37% survival probability for particles with size d_0. ψ represents Weibull modulus which is material dependent. The lower the ψ, the larger variation in particle strength. Typical values of Weibull modulus for silica sand vary in the range of approximately 1 to 4 [77-79]. For sand with relatively high purity, such as quartz sand, a relatively large Weibull modulus can be expected. On the other hand, sand containing mixture of minerals often exhibit small Weibull modulus, indicating large variations in particle strength. In this study we assume a typical Weibull modulus of 3.1 for numerical modeling [60]. Implementation of Weibull statistics on particle strength consists of two procedures, one pertains to assigning strengths to particles in the initial packing, the other addresses the size effect when particles crush and evolve into smaller ones. The two procedures are discussed in Sections 4.2 and 4.3, respectively.

4.2 Particle strength in the initial packing

The survival probability curves for various size of quartz sand particles are shown in Fig. 8 where particle strengths are normalized by a characteristic strength of the same size [8,78]. The figure indicates that particle size (at least within the tested range) does not impose apparent influence on the normalized strength. In our modeling, similar to the approach used by Hanley et al. [80], a linear simplification to the survival probability curve is considered as shown in Fig. 8. For each particle in the initial packing, a unique strength can be assigned following Eq. (12), where d_0 and σ_0 represent the size and characteristic strength of a reference particle, a and b are the slope and vertical intercept of the simplified survival probability curve, which have been determined to be -0.76 and 1.13, respectively. $U(0,1)$ represents a random number between 0 and 1 drawn from a uniform distribution.

$$\sigma = \sigma_0 \frac{U(0,\ 1) - b}{a}\left(\frac{d}{d_0}\right)^{-\frac{3}{\psi}} \tag{12}$$

Accepted Manuscript

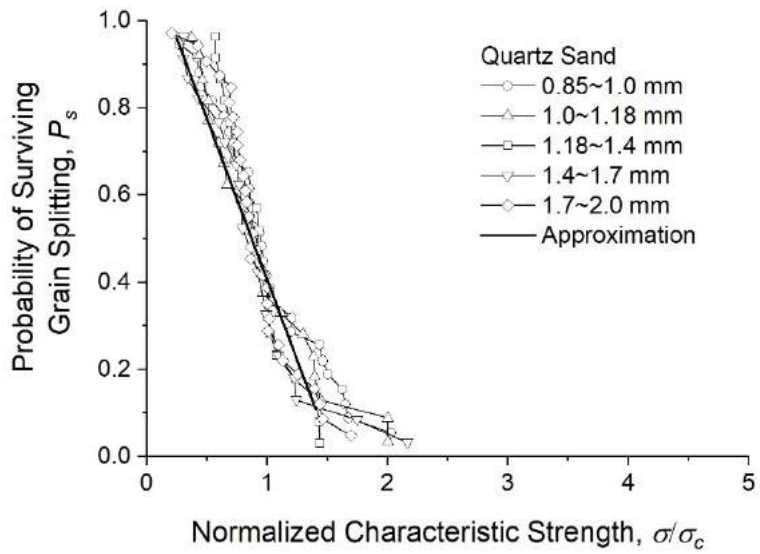

Fig. 8. Normalized survival probability of quartz sand particles and approximation.

In peridynamic analysis, nonetheless, the strength of a particle is quantified by the critical energy release rate G_c. Particles with different strengths can be modeled by assigning different G_c values. Larger G_c represents stronger material since more energy is required to create new material surfaces and vice versa. A relationship between the characteristic strength σ and G_c must be established for implementation of Eq. (12) in peridynamic analysis. Such relationship may be found from a "classical" scenario where a particle crushes under uniaxial loadings. In such scenario, the characteristic strength σ is proportional to the maximum crushing force on the particle which bears a linear relation to maximum tensile stress inside the particle [81]. The maximum tensile stress is proportional to the maximum tensile strain ε_t for a linear elastic material. The ε_t is essentially proportional to the critical stretch (maximum allowed strain of a peridynamic bond) which is related to G_c through Eq. (5). Therefore, it is not difficult to deduce that the characteristic strength of a particle, σ, is proportional to the square root of G_c for a given particle. The relation may be expressed by $\sigma \propto \sqrt{G_c}$, and Eq. (14) can be rewritten as:

$$G_c = G_{c0}\left(\frac{U(0,\ 1) - b}{a}\right)^2 \left(\frac{d}{d_0}\right)^{-\frac{6}{\psi}} \tag{13}$$

where G_c and G_{c0} represent critical energy release rate of particles with size d and d_0, respectively. G_{c0} and d_0 should be known values and serve as a reference based on which the strengths of particles are defined. Favourably, G_{c0} and d_0 should be determined or calibrated based on experimental studies to ensure that the assigned strengths are realistic reflection of natural material properties. In the present study, we adopt G_{c0} = 30 J/m^2 for a particle with d_0 = 2.0 mm as the reference case. Under such case, a peridynamic simulation of uniaxial compression of the particle yields a characteristic strength near 45 MPa which agree well with experimental records for typical silica sand [60]. With such reference established, the strength of each particle in the initial packing can be assigned following Weibull distribution using Eq. (13). The breakage analysis threshold mentioned in Section 3.1 is also assigned to each particle based on Eq. (12).

Accepted Manuscript

The relation of $\sigma \propto \sqrt{G_c}$ is critical in establishment of Eq. (13). As a verification to such relation, a series of peridynamic simulations of uniaxial particle crushing were performed. The simulations were set up with the techniques introduced in Section 3. A base case is selected for a particle with 2.0 mm diameter and G_{c0} = 30 J/m^2, which yields a crushing force of about 180 N in the simulation, corresponding to a characteristic strength near 45 MPa. Prediction of particle strength following the relationship of $\sigma \propto \sqrt{G_c}$ is shown in Fig. 9 by the dashed line. Simulations are then performed for cases where G_c = 5, 10, 20, 40, and 50 J/m^2. Good agreement can be observed between the simulation results and theoretical prediction while the slight deviation may be explained by the simplified contact model we adopted. The simulations further confirm the validity of the relation we established between σ and G_c.

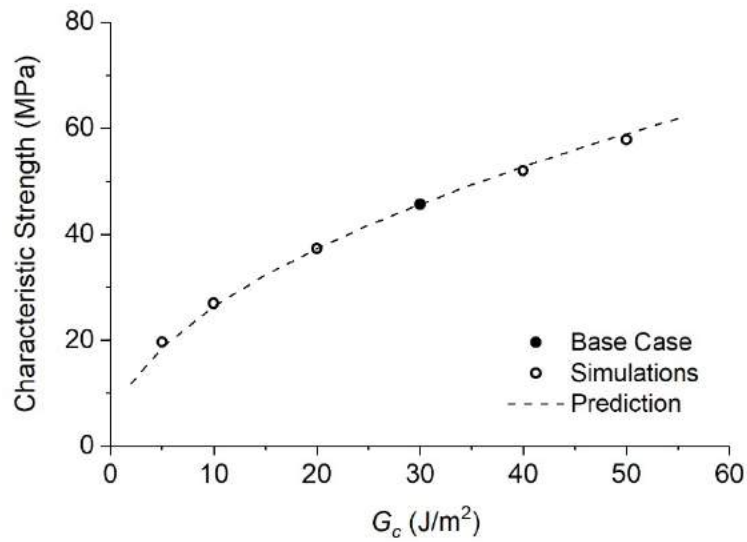

Fig. 9. Verification of relationship between G_c and σ by peridynamic analysis of a particle crushed under uniaxial loadings.

4.3 Size effect on particle strength

Crushing of particle results in reduction in particle size. The Weibull's weakest link theory [82] points out that large particles are more prone to crushing since they tend to contain more and bigger defects, whereas small particles in general contain less and smaller defects. Consequently, small particles tend to be stronger than large particles. When crushing occurs to a particle, such size effect needs to be quantified. Nakata et al. [78] have shown that the characteristic strengths of particles with different sizes observe the following relation:

$$\frac{\sigma_a}{\sigma_b} = \left(\frac{d_a}{d_b}\right)^{-\frac{3}{\psi}} \tag{14}$$

where σ_a and σ_b represent characteristic strength of two particles a and b with equivalent size of d_a and d_b, respectively. If we consider particle a as a child particle of its parent particle b and incorporate the relation between σ and G_c, Eq. (14) can be rewritten as:

Accepted Manuscript

$$G_{c-ch} = G_{c-pr}\left(\frac{d_{ch}}{d_{pr}}\right)^{-\frac{6}{\psi}} \tag{15}$$

where $G_{c\text{-}ch}$ and $G_{c\text{-}pr}$ represent critical energy release rates for the child particle and parent particle, respectively. d_{ch} and d_{pr} represent the size of child particle and parent particle, respectively. Eq. (15) is used to assign strength to each child particle formed from breakage. The breakage analysis threshold as mentioned in Section 3.1 is assigned to each child particle following Eq. (14).

It needs to be mentioned that the quantification of particle strength following Eqs. (13) & (15) inherently assumes that the characteristic strength of a particle is solely decided by the critical energy release rate. However, the formulation presented in Eq. (5) brings a certain (and unwanted) size effect since the critical stretch is determined by both G_c and the horizon δ which is proportional to the size of particle. It is not difficult to discern that such formulation indicates a relation of $\sigma \propto \sqrt{G_c/d}$ instead of $\sigma \propto \sqrt{G_c}$. Therefore, we further modify the critical stretch of particles in peridynamic analysis by implementing:

$$s_c = s_{c(ref)}\sqrt{\frac{d}{d_{ref}}} \tag{16}$$

where $s_{c(ref)}$ represents critical stretch calculated using Eq. (5) for the reference particle (e.g., with d_{ref} = 2.0 mm). Implementing Eq. (16) ensures that characteristic strength of a particle is solely a function of G_c. The purpose of such modification is to support the implementation of Weibull statistics on particle strength for natural granular materials. The modification does not imply any fundamental change to the peridynamics theory presented in Section 2 and should only be applied for the specific purpose.

5. Simulation of 1-D compression of sand

A 1-D compression of sand is simulated using the presented numerical framework. The sand sample consists of initially 720 spherical particles packed in a rigid box having a dimension of 13.6 mm by 13.6 mm and a height of about 14 mm with smooth boundaries. The initial sample is slightly polydispersed and consists of particles with diameters ranging from 1.4 mm to 2.0 mm. The particle size distribution (PSD) is shown in Fig. 10. The PSD is similar to that adopted in a 1-D compression experiment performed by McDowell [60] to ease subsequent comparisons. The initial packing was generated by two steps. First, a "cloud" of particles is generated inside the rigid box and the sizes of particles are assigned randomly following the PSD. Then, the particles are pushed by a rigid plate with a small force from top towards bottom of the rigid box until a stable packing is formed. The initial void ratio of the generated packing is about 0.71. The parameters of sand adopted for the analysis are summarized in Table 1.

Vertical pressure is applied on a rigid platen modeled at top of the sample by a stress-controlled mode. The pressure is set to increase linearly with time up to 30 MPa with a duration of 0.15 s. Time step has been chosen according to the pressure level, considering the fact that particle size generally reduces with increasing load which calls for smaller time step for better

Accepted Manuscript

accuracy. In current study, a time step of 8×10^{-5} s, 6×10^{-5} s, and 5×10^{-5} s is used for vertical pressure below 10 MPa, between 10 MPa and 24 MPa, and above 24 MPa, respectively. Breakage of particles is checked at every 0.08 MPa pressure increment. As a common practice, a crushing limit is also set in the model at 0.3 mm. In other words, a particle with equivalent diameter less than 0.3 mm will not be analyzed for breakage. The continuous crushing process of the sample may not be a strict quasi-static process since the particles move and rearrange themselves during the loading process. It is assumed in this study that those particles in motion will not undergo crushing. Numerical wise, particles possessing an unbalanced force ratio above 0.02 or an unbalanced moment ratio above 0.2 are considered in motion and are not selected for breakage analysis. The unbalanced force ratio is calculated by the ratio of unbalanced force on a particle to the average force magnitude on that particle. Similarly, the unbalanced moment ratio is defined as the ratio of unbalanced moment on a particle about the point of fixity to the average magnitude of moment on that particle. To enhance stability of the simulation, the mass of the modeled particles are amplified by 70 times. Such magnitude of mass scaling has been carefully checked to avoid bringing inertia effect into the simulation. If a higher mass scaling is applied, the time step may be taken larger but the duration of simulation also needs to be longer to avoid inertia effect.

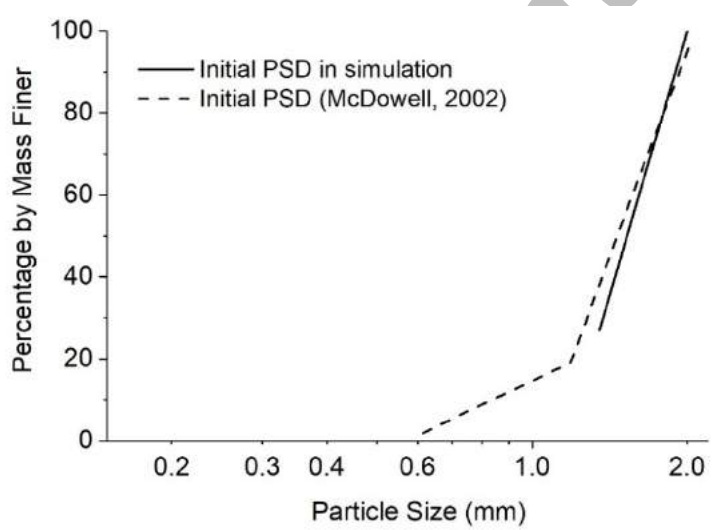

Fig. 10. Initial particle size distribution of the simulated sample.

Table 1. Summary of adopted parameters of sand in simulation

Parameter	Value
Density (kg/m^3)	2650
Young's modulus (GPa)	100
Poisson's ratio	0.15
Critical energy release rate (J/m^2) (base case for a 2 mm dia. particle with characteristic strength of 45 MPa)	30
Weibull modulus	3.1

Inter-particle friction coefficient	0.5
Particle-wall friction coefficient	0.0
Rolling friction coefficient	0.05
Restitution	0.0

In peridynamic analysis, when boundary conditions are applied on particles, the forces are set to increase linearly with time and the loading rate is selected according to particle size. We perform a set of simulations of uniaxial crushing of spherical particles with sizes ranging from 0.5mm to 2.0mm to determine the appropriate loading rate in peridynamics. As shown in Fig. 11, the failure load generally exhibits an increasing trend with higher loading rates. Large particles appear to be less sensitive to loading rate, allowing selection of higher loading rates without causing apparent influence on the failure force level. Small particles, on the other hand, are less tolerant to the increase of loading rate. In the simulation we have selected the loading rate to be 2.0×10^6 N/s, 1.2×10^6 N/s, and 1.0×10^6 N/s for particles with equivalent diameter d_e of 1.0 ~ 2.0 mm, 0.6 ~ 1.0 mm, and below 0.6 mm, respectively. The selected loading rates aim to maximize computational speed in peridynamic analysis. The failure force level may be affected slightly as a result of elevated loading rate, but they still represent realistic strengths of sand particles. The breakage patterns are also checked and found not affected by the selected loading rates. For the presented simulation, the computational time is approximately 200 hours if run on a desktop with 4 CPUs at 3.5 GHz. The time can be greatly reduced if more computing power is available. For instance, with 36 CPUs at the same frequency we would estimate a 40% to 50% saving in computing time. It should be noted that there remain large room for further improvement of the computational efficiency by parallelizing the discrete modeling in physics engine, which we intend to address in a separate study.

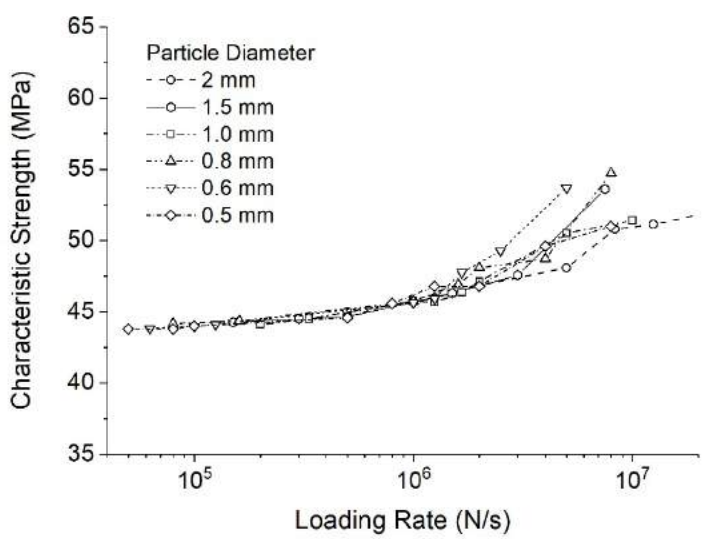

Fig. 11. Loading rate effect on characteristic strength of single particles under uniaxial loadings.

Accepted Manuscript

The normal compression line (NCL) obtained from the simulation is presented in Fig. 12. Together shown is the number of crushing events recorded in the simulation at different vertical stress levels. At low stress levels (i.e., 0 ~ 3 MPa), no crushing event was recorded in the simulation due to the small contact forces experienced by the particles. With increasing stress levels (i.e., 4 ~ 10 MPa), tens to about a hundred particles experienced crushing during each 1 MPa stress increment, and the NCL shows apparent curvature which reflects the void reduction resulted from crushing and rearrangement of particles. Yielding of the sample may be defined at stress levels of 6 MPa to 8 MPa. Further increasing the stress level led to significant particle crushing in the sample. At stresses above 20 MPa, the number of particles experienced crushing surged to 500 ~ 600 in each 1 MPa increment. The recorded NCL is approximately linear when plotted in a log-log space, with a slope of approximately 0.52 which agree reasonably with past experimental and analytical studies [60,83]. The recorded number of particles in the simulation versus vertical pressure is shown in Fig. 13. The number of particles increases apparently at yielding of the sample, and then starts to increase exponentially. At the end of the simulation, the number of particles is approximately 27,400, which is nearly 40 times the number of particles at the beginning of the simulation. The observation again implies a high computational cost for both breakage analysis and discrete modeling at large stress levels. The simulated sand sample at difference loading levels are visualized in Fig. 14. At a stress level of 5 MPa, only a few particles are noticed to experience crushing. With increasing stress, more particles in the initial packing experienced crushing and some broken pieces have experienced continuous crushing. At high stress levels (e.g., 20 ~ 30MPa), many particles have gone through several crushing events and formed small pieces filling the voids between large particles. Some large particles are preserved even at the stress level of 30 MPa, probably due to the cushion effect from the surrounding small particles which mitigates stress and force concentration on those large ones [11]. The particle size distributions at selected stress levels are shown in Fig. 15 where reasonable agreement can be observed between simulation results and experimental records.

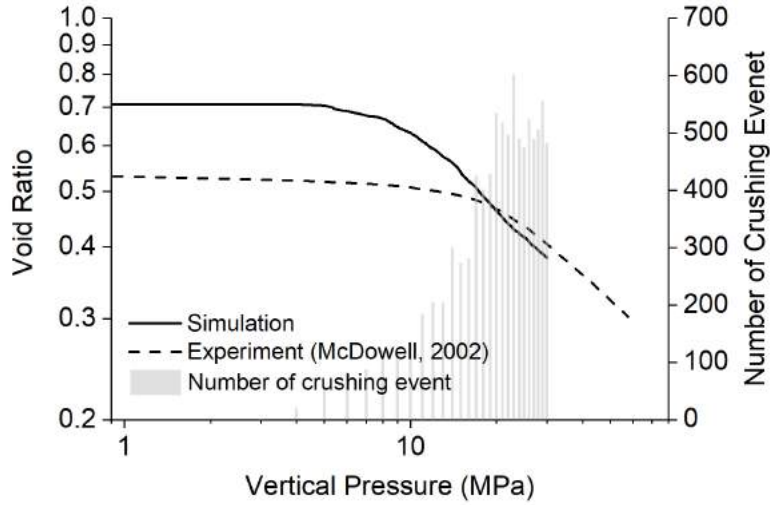

Fig. 12. Normal compression line obtained from simulation.

Accepted Manuscript

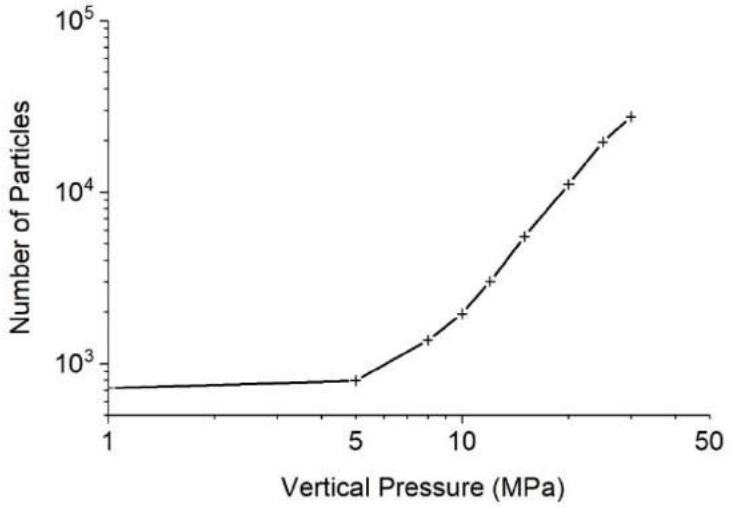

Fig. 13. Number of particles in the sample at different loading levels.

Accepted Manuscript

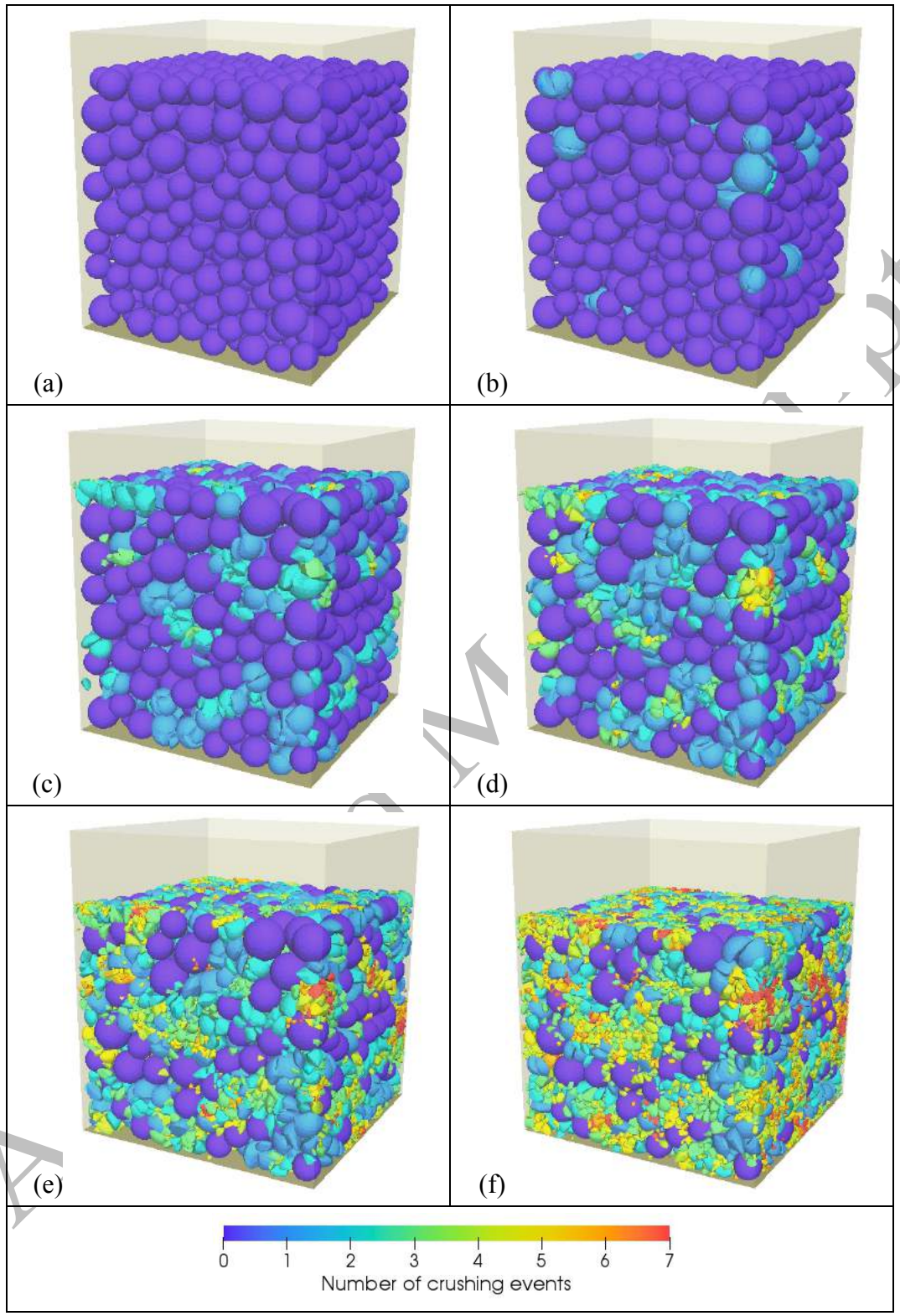

Fig. 14. Simulated sand sample at different vertical pressures. (a) initial condition; (b) σ_v = 5 MPa; (c) σ_v = 10 MPa; (d) σ_v = 15 MPa; (e) σ_v = 20 MPa; (f) σ_v = 30 MPa. The color indicates the number of crushing events experienced by a particle.

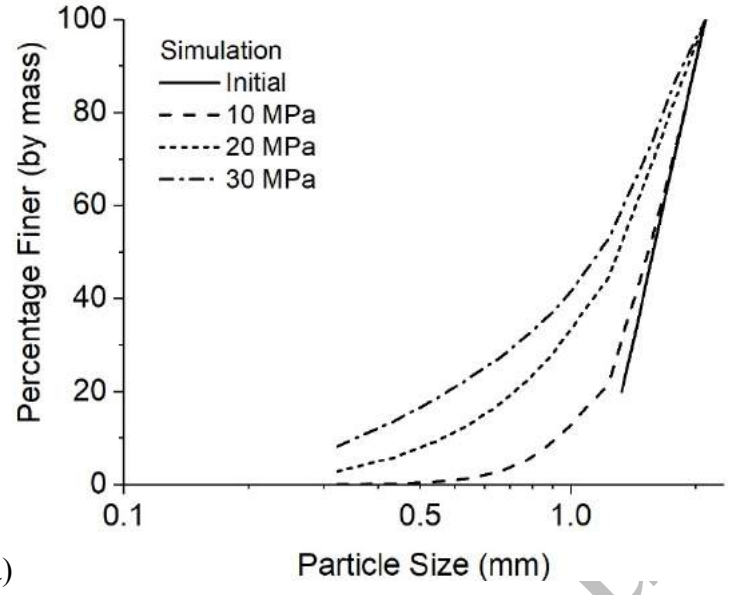

(a)

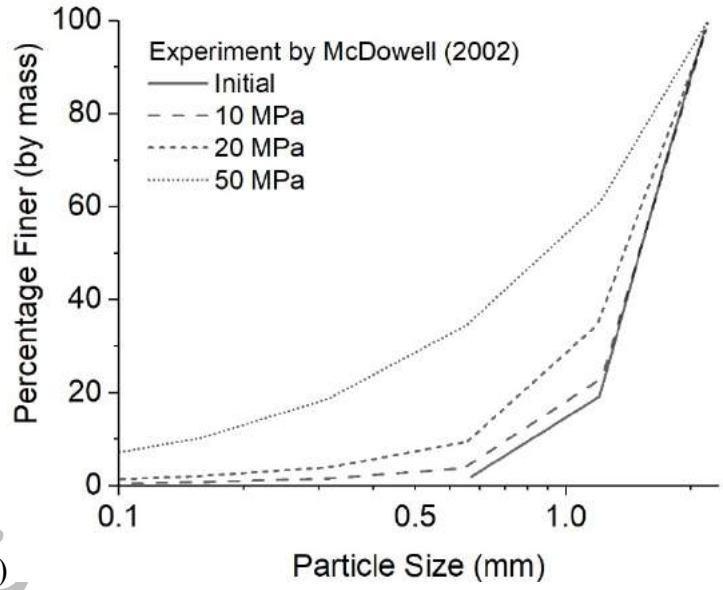

(b)

Fig. 15. Evolution of particle size distribution obtained from simulation (a) and comparison with experimental results (b).

As a naturally occurring material, sand follows a scale invariant process during its fragmentation which can be described by the concept of fractal [54,84]. The size of sand particles is known to follow a fractal distribution, which defines the number of particles with size larger than d_0 to have a power law relation to the size d_0 as presented by:

$$N(d > d_0) \propto {d_0}^{-D} \tag{17}$$

where D is known as fractal dimension. Various studies [54,56,59] have suggested a fractal dimension ranging from slightly below 2.0 to near 3.0 for natural sand. The fractal dimension is

obtained from simulation results by plotting N ($d > d_0$) versus d_0 in a log-log space as shown in Fig. 16. The slope of those lines, which indicates fractal dimension at different loading levels, are summarized and plotted in Fig. 17. It is clearly indicated that the fractal dimension raises with increasing load and stays nearly constant at a reasonable value of approximately 2.3.

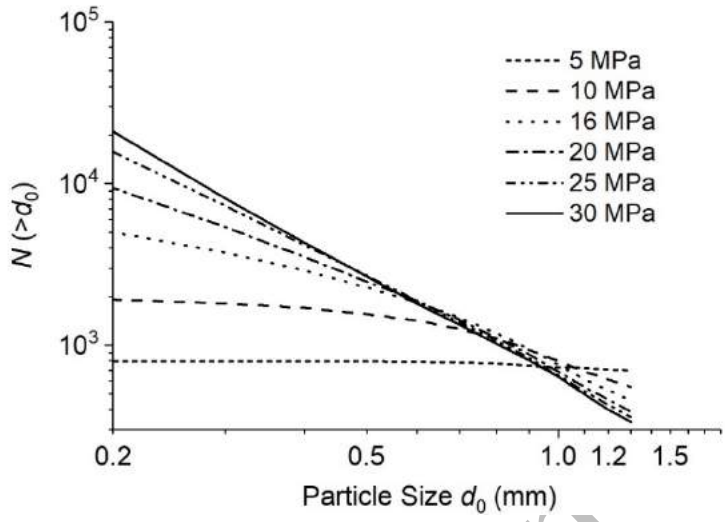

Fig. 16. Particle size distribution plotted in N (with $d > d_0$) versus d_0.

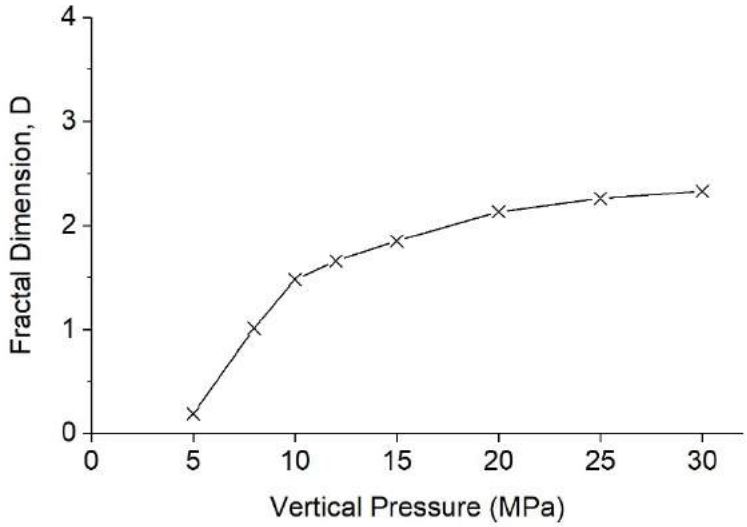

Fig. 17. Fractal dimension evolution with increasing vertical pressure.

We further extend the study to examine the shape of particles formed in the crushing process. This field was poorly explored in the past as the traditional spherical particle DEM was incapable to quantify particle shapes with reasonable accuracy and other methods were not efficient enough to generate statistically meaningful results. The shape of a particle may be quantified by various parameters such as sphericity, convexity, elongation, flatness, aspect ratio, and roughness. In this study we only examine two essential particle shape features: flatness index (FI) and elongation index (EI). Other features of the particles may be studied with more detailed modeling of particle surface morphology and is beyond the scope of current study. The FI and EI

can be calculated by FI = S/I and EI = I/L, where S, I, L represent short, intermediate, and long dimension of a particle, respectively. Here we use a principal axis approach [85-86] to define the three dimensions of a particle. For each particle, the principal axes of inertia are found first and the particle is rotated so that the principal axes of inertia coincide with the Cartesian coordination axes. The dimensions S, I, L correspond to the minimum, intermediate, and maximum expansion on the three Cartesian directions, respectively. The shapes of simulated particles are shown in a Zingg diagram in Fig. 18 at vertical pressures of 10, 15, 20, and 30 MPa. The diagram clearly indicates that particles undergone crushing tend to possess EI and FI both between 0.5 and 1.0. A large portion of the particles fall within the category of "*spheroid*" in the classification by Zingg [87]. Particles having EI below 0.4 (i.e., highly elongated) or FI below 0.4 (i.e., thin shape) are rare since they are prone to breakage and are unlikely to survive through continuous breakage process. Experimental measurement on the elongation and flatness of sand particles is very limited. Nonetheless, three sets of experimental records are obtained from literatures and are presented in Fig. 18 for comparison. Among them, Fonseca et al. [85] measured samples of Reigate sand particles which is formed by cemented quartz mineral. Zhao et al. [59] measured a few Leighton Buzzard sand (LBS, a type of silica sand) and highly decomposed granite sand particles. The measurements by Zhao & Wang [86] are also for LBS particles and two subsets of data are available, corresponding to the original particles selected for crushing tests and the broken pieces from single particle crushing tests, respectively. The experimental measurements indicate that both EI and FI of the sand particles fall most likely between 0.5 and 1.0, and within the "*spheroid*" region, which confirm the simulation results of particle shapes with respect to flatness and elongation. For the particles that undergone single particle crushing test (e.g., the crushed particles in Zhao & Wang [86]), lower values of EI and FI were observed in experiment. This is not surprising as particles undergone one or a few crushing events under uniaxial loading is likely elongated or flat. If those broken pieces are placed in the context of granular media and undergone a continuous breakage process, those elongated or flat particles will likely diminish.

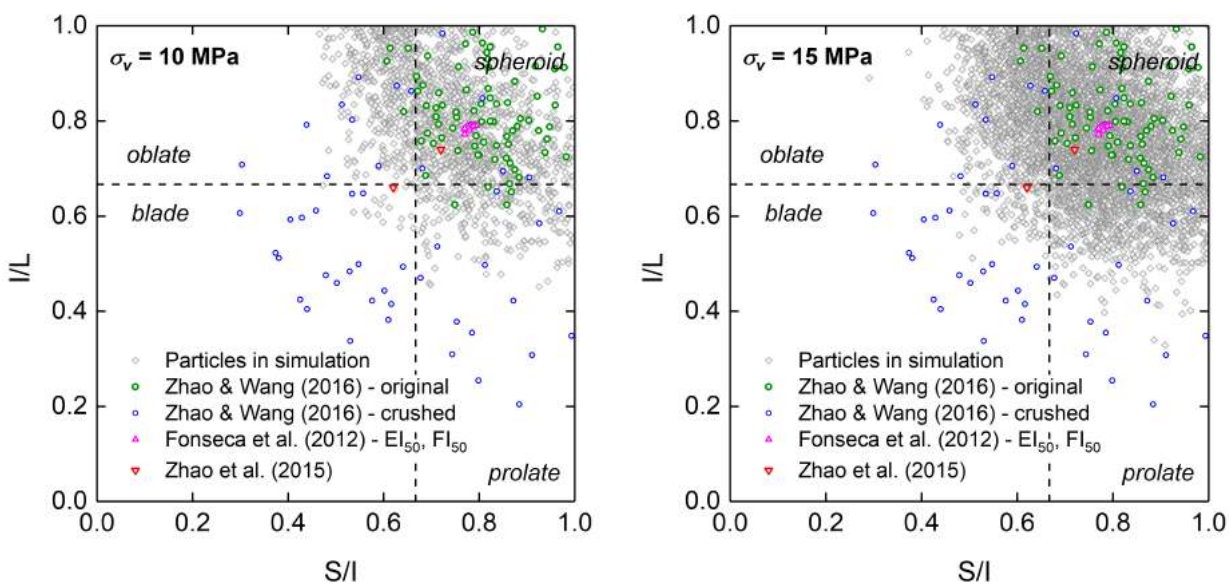

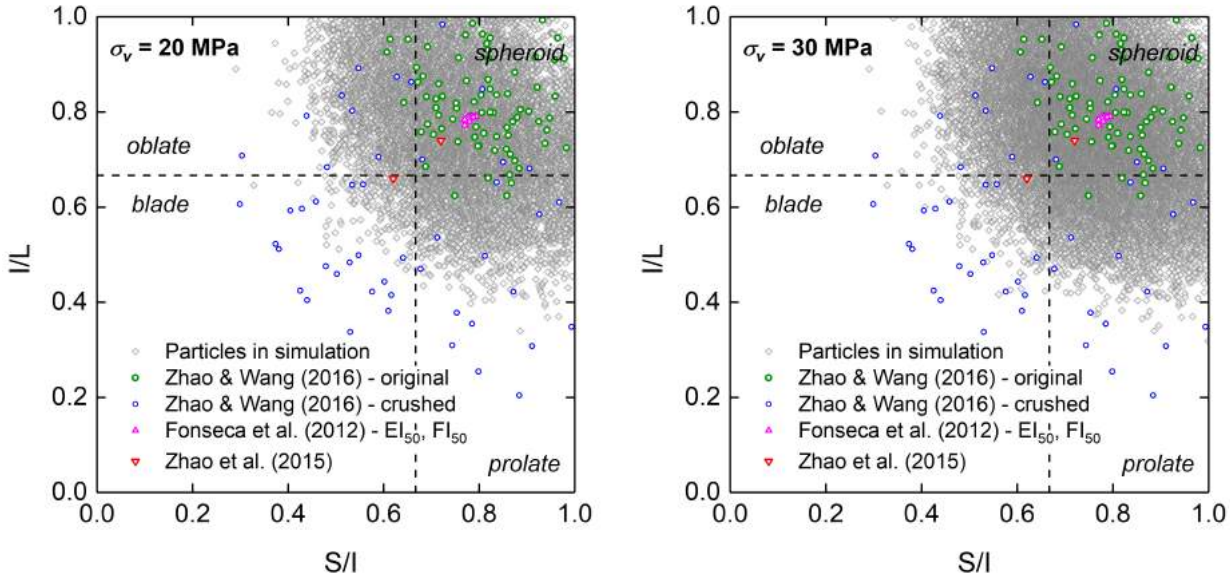

Fig. 18. Zingg diagram of simulated particles at 10 MPa, 15 MPa, 20 MPa, 30 MPa and comparison with experimental records.

The simulation therefore confirms the capability of the proposed numerical framework in predicting reasonable macroscopic behavior of crushable granular sand under 1-D compression. It may also be desirable to review the simulation results from a microscopic perspective by comparison with experimental measurements on microscopic behaviours such as crack patterns and fabric structures. The microscopic measurement on crushable granular material is often aided by scanning electron microscope (SEM) or X-Ray scanning techniques. Nonetheless, relevant experimental works remain limited for an in-depth comparison at the moment, and a separate study focusing on microscopic aspects will be performed in a later stage.

6. Conclusions and outlook

In this paper we presented a novel hybrid computational framework combining peridynamics and a CD-based physics engine for modeling crushable granular material. Also introduced is a strategy to implement Weibull statistical distribution on particle strength for natural materials. The framework utilizes peridynamics for analyzing crushing of individual particles and physics engine for modeling granular system. The framework is advantageous over traditional methods in the sense that continuous particle breakage is rigorously modeled and irregular particle shapes are handled. Simulation of 1-D compression of a sand sample has been presented which demonstrated that the proposed numerical framework produced reasonable results with respect to particle size distribution, fractal dimension, normal compression, as well as particle morphology. The proposed computational framework offers a pathway to investigate many aspects of micro-mechanical behaviour of crushable granular materials, such as particle shape evolutions, fabric structure, particle crushing conditions and fracture pattern, and energy consumption in the crushing process. Based on new sights derived from these aspects, key theories and concepts governing continuum mechanics of crushable sands, such as shear strength [88-89], critical state

Accepted Manuscript

[90-92], dilatancy and fabric evolution [93-95], can all be reassessed and reformulated for better understanding and prediction of material crushing. The entire algorithm proposed in the study can also be conveniently embedded into the recently prevailing hierarchical multiscale framework [96-99] for cross-scale modeling of geomechanics problems. Although the presented simulation focused on geomaterials, it is never the intention of the authors to restrict the application of the method within geotechnical discipline. The framework may be further developed to simulate a variety of industrial processes such as grinding, comminution, mechanical crusher processing, and transportation and piling of industrial granular matter.

The presented work is not without limitations, and future improvements may be made from several aspects: 1) the material in current study has been assumed to be isotropic and homogeneous in peridynamic analysis while anisotropic and heterogeneous materials widely exist in nature, which may lead to different crushing behaviours. The crushing of granular material may also experience influence from stress history, fluid, and temperature change. These scenarios may require more complex material models to be implemented as well as multi-phase modeling; 2) the presented simulation has simplified the particle morphology to some extent for the sake of computational efficiency. Small fragments formed from breakage were not modeled. Detailed modeling of particle surface morphology and the fragments require more powerful computing facility in discrete modeling. A GPU level parallel computing approach appears to be attractive for future enhancement on computational efficiency. More advanced techniques for solving constraint system in physics engine may also be studied to further improve computational efficiency and accuracy.

Acknowledgements

The study was financially supported by National Natural Science Foundation of China (via Project No. 51679207) and Research Grants Council of Hong Kong under the General Research Fund (via Project No. 16210017), the Theme-based Research Scheme (via Project No. T22-603/15-N) and the Collaborative Research Fund scheme (via Project No. C6012-15G). The first author acknowledges financial support from Hong Kong Ph.D. Fellowship Scheme funded by Research Grants Council of Hong Kong.

Accepted Manuscript

References

[1] B.O. Hardin, Crushing of soil particles, Journal of Geotechnical Engineering 111 (10) (1985) 1177-1192.

[2] G.R. McDowell, M.D. Bolton, On the micromechanics of crushable aggregates, Géotechnique 48 (5) (1998) 667–679.

[3] P.V. Lade, J.A. Yamamuro, P.A. Bopp, Significance of particle crushing in granular materials, Journal of Geotechnical Engineering 122 (4) (1996) 309-316.

[4] P.A. Cundall, O.D.L. Strack, A discrete numerical model for granular assemblies, Géotechnique 29 (1) (1979) 47-65.

[5] Y.P. Cheng, Y. Nakata, M.D. Bolton, Discrete element simulation of crushable soil, Géotechnique 53 (7) (2003) 633-641.

[6] M.B. Cil, K.A. Alshibli, 3D assessment of fracture of sand particles using discrete element method, Géotechnique Letters 2 (3) (2012) 161-166.

[7] P. Wang, C. Arson, Discrete element modeling of shielding and size effects during single particle crushing, Computers and Geotechnics 78 (2016) 227-236.

[8] J. Wang, H. Yan, On the role of particle breakage in the shear failure behavior of granular soils by DEM, International Journal for Numerical and Analytical Methods in Geomechanics 37 (8) (2013) 832–854.

[9] G.R. McDowell, J.P. de Bono, On the micro mechanics of one-dimensional normal compression, Géotechnique 63 (11) (2013) 895-908.

[10] J.P. de Bono, G.R. McDowell, DEM of triaxial tests on crushable sand, Granular Matter 16 (4) (2014) 551-562.

[11] J.P. de Bono, G.R. McDowell, Particle breakage criteria in discrete-element modelling, Géotechnique 66 (12) (2016) 1014-1027.

[12] J.P. de Bono, G.R. McDowell, Micro mechanics of drained and undrained shearing of compacted and overconsolidated crushable sand, Géotechnique 68 (7) (2018) 575-589.

[13] S. Lobo-Guerrero, L. Vallejo, Crushing a weak granular material: experimental numerical analyses, Géotechnique 55 (3) (2005) 245-249.

[14] T. Brosh, H. Kalman, A. Levy, Fragments spawning and interaction models for DEM breakage simulation, Granular Matter 13 (6) (2011) 765-776.

[15] G.C. Cho, J. Dodds, J.C. Santamarina, Particle shape effects on packing density, stiffness, and strength: natural and crushed sands, Journal of Geotechnical and Geoenvironmental Engineering 132 (5) (2006) 591–602.

[16] P.A. Cundall, Formulation of a three-dimensional distinct element model - Part I. A scheme to detect and represent contacts in a system composed of many polyhedral blocks, Int. J. Rock Mech. Min. Sci. & Geomech. Abstr. 25 (3) (1988) 107-116.

[17] J. Elias, Simulation of railway ballast using crushable polyhedral particles, Powder Technology 264 (2014) 458-465.

Accepted Manuscript

[18] D. Hohner, S. Wirtz, H, Kruggel-Emden, V. Scherer, Comparison of the multi-sphere and polyhedral approach to simulate non-spherical particles within the discrete element method: Influence on temporal force evolution for multiple contacts, Powder Technology 208 (3) (2011) 643-656.

[19] S.J. Lee, Y.M.A. Hashash, E.G. Nezami, Simulation of triaxial compression tests with polyhedral discrete elements, Computers and Geotechnics 43 (2012) 92-100.

[20] J. Wang, H.S. Yu, P. Langston, F. Fraige, Particle shape effects in discrete element modelling of cohesive angular particles, Granular Matter 13 (1) (2011) 1-12.

[21] A. Gladkyy, M. Kuna, DEM simulation of polyhedral particle cracking using a combined Mohr–Coulomb–Weibull failure criterion, Granular Matter 19 (3) (2017) 41.

[22] F. Nader, C. Silvani, I. Djeran-Maigre, Grain breakage under uniaxial compression using a three-dimensional discrete element method, Granular Matter 19 (3) (2017) 53.

[23] D.H. Nguyen, E. Azéma, P. Sornay, F. Radjai, Bonded-cell model for particle fracture, Phys. Rev. E 91 (2) (2015) 022203.

[24] R. Kawamoto, E. Andò, G. Viggiani, J.E. Andrade, Level set discrete element method for three-dimensional computations with triaxial case study, Journal of the Mechanics and Physics of Solids 91 (2016) 1-13.

[25] A. Munjiza, D.R.J. Owen, N. Bicanic, A combined finite-discrete element method in transient dynamics of fracturing solids, Engineering Computations 12 (2) (1995) 145-174.

[26] A. Munjiza, The Combined Finite-Discrete Element Method (2004) John Wiley & Sons Ltd, Chichester, England.

[27] G. Ma, W. Zhou, X.L. Chang, M.X. Chen, A hybrid approach for modeling of breakable granular materials using combined finite-discrete element method, Granular Matter 18 (1) (2016) 7.

[28] G. Ma, W. Zhou, R.A. Regueiro, Q. Wang, X. Chang, Modeling the fragmentation of rock grains using computed tomography and combined FDEM, Powder Technology 308 (2017) 388-397.

[29] A.B. Kh., A.A. Mirghasemi, S. Mohammadi, Numerical simulation of particle breakage of angular particles using combined DEM and FEM, Powder Technology 205 (1–3) (2011) 15-29.

[30] J. Raisianzadeh, A.A. Mirghasemi, S. Mohammadi, 2D simulation of breakage of angular particles using combined DEM and XFEM, Powder Technology 336 (2018) 282-297.

[31] Y.J. Ning, X.M. An, Q. Lü, G.W. Ma, Modeling rock failure using the numerical manifold method followed by the discontinuous deformation analysis, Acta Mechanica Sinica 28 (3) (2012) 760-773.

[32] S.B. Tang, R.Q. Huang, C.A. Tang, Z.Z. Liang, M.J. Heap, The failure processes analysis of rock slope using numerical modelling techniques, Engineering Failure Analysis 79 (2017) 999-1016.

[33] S.A. Silling, Reformulation of elasticity theory for discontinuities and long-range forces, Journal of the Mechanics and Physics of Solids 48 (1) (2000) 175-209.

Accepted Manuscript

[34] S.A. Silling, M. Epton, O. Weckner, J. Xu, A. Askari, Peridynamics states and constitutive modeling, Journal of Elasticity 88 (2) (2007) 151–184.

[35] X.P. Zhou, Y.D. Shou, Numerical simulation of failure of rock-like material subjected to compressive loads using improved peridynamic method, International Journal of Geomechanics 17 (3) (2017) 04016086.

[36] B. Kilic, E. Madenci, Prediction of crack paths in a quenched glass plate by using peridynamic theory, International Journal of Fracture 156 (2) (2009) 165–177.

[37] F. Zhu, J. Zhao, A peridynamic investigation on crushing of sand particles, Géotechnique (2018) doi: 10.1680/jgeot.17.p.274.

[38] X. Lai, B. Ren, H. Fan, S. Li, C.T. Wu, R.A. Regueiro, L. Liu, Peridynamics simulations of geomaterial fragmentation by impulse loads. International Journal for Numerical and Analytical Methods in Geomechanics 39(12) (2015) 1304-1330.

[39] M. Jean, The non-smooth contact dynamics method, Computer Methods in Applied Mechanics and Engineering 177 (3-4) (1999) 235-257.

[40] F. Radjai, V. Richefeu, Contact dynamics as a nonsmooth discrete element method, Mechanics of Materials 41 (6) (2009) 715-728.

[41] E. Coumanns, Bullet physics library (version 2.87), http://bulletphysics.org (2017).

[42] A. Tasora, R. Serban, H. Mazhar, A. Pazouki, D. Melanz, J. Fleischmann, M. Taylor, H. Sugiyama, D. Negrut, Chrono: An open source multi-physics dynamics engine. In T. Kozubek, editor, High Performance Computing in Science and Engineering – Lecture Notes in Computer Science (2016) 19–49. Springer.

[43] E. Catto, Box2d: A 2d Physics Engine for Games, http://box2d.org (2011).

[44] M. Pytlos, M. Gilbert, C.C. Smith, Modelling granular soil behaviour using a physics engine, Géotechnique Letters 5 (4) (2015) 243-249.

[45] R. Smith, Open Dynamics Engine v0.5 User Guide. http://ode.org (2006).

[46] E. Izadi, A. Bezuijen, Simulation of granular soil behaviour using the bullet physics library, In Geomechanics from micro to macro (2015) 1565-1570. London, UK: Taylor & Francis Group.

[47] E. Izadi, A. Bezuijen, Simulating direct shear tests with the Bullet physics library: A validation study, PLoS ONE 13 (4) (2018) e0195073.

[48] P. Toson, J.G. Khinast, Impulse-based dynamics for studying quasi-static granular flows: Application to hopper emptying of non-spherical particles, Powder Technology 313 (2017) 353-360.

[49] S.J. Lee, Y.M.A. Hashash, iDEM: An impulse-cased discrete element method for fast granular dynamics, International Journal for Numerical Methods in Engineering 104 (2015) 79-103.

[50] Y.T. Feng, K. Han, D.R.J. Owen, Energy-conserving contact interaction models for arbitrarily shaped discrete elements, Computer Methods in Applied Mechanics and Engineering 205-208 (2012) 169-177.

Accepted Manuscript

[51] A. Munjiza, K.R.F. Andrews, Penalty function method for combined finite-discrete element systems comprising large number of separate bodies, International Journal for Numerical Methods in Engineering 49 (11) (2000) 1377-1396.

[52] B. Smeets, T. Odenthal, S. Vanmaercke, H. Ramon, Polygon-based contact description for modeling arbitrary polyhedra in the Discrete Element Method, Computer Methods in Applied Mechanics and Engineering 290 (2015) 277–289.

[53] M. Servin, D. Wang, C. Lacoursière, K. Bodin, Examining the smooth and nonsmooth discrete element approaches to granular matter, Int. J. Numer. Meth. Engng. 97 (12) (2014) 878–902.

[54] D.L. Turcotte, Fractals and fragmentation, Journal of Geophysical Research 91 (B2) (1986) 1921–1926.

[55] A.C. Palmer, T.J.O. Sanderson, Fractal crushing of ice and brittle solids, Proc. R. Soc. Lond. A 433 (1889) (1991) 469–477.

[56] G.R. McDowell, M.D. Bolton, D. Robertson, The fractal crushing of granular materials. Journal of the Mechanics and Physics of Solids 44 (12) (1996) 2079–2101.

[57] M.L. Parks, D.J. Littlewood, J.A. Mitchell, S.A. Silling, Peridigm Users' Guide, Sandia Report, Sandia National Laboratories. Albuquerque, NM, USA, 2012.

[58] E. Madenci, E. Oterkus, Peridynamic Theory and Its Applications, Springer, New York, 2014.

[59] B. Zhao, J. Wang, M.R. Coop, G. Viggian, M. Jiang, An investigation of single sand particle fracture using X-ray micro-tomography, Géotechnique 65 (8) (2015) 625-641.

[60] G.R. McDowell, On the yielding and plastic compression of sand, Soils and Foundations 42 (1) (2002) 139-145.

[61] X. Lai, L. Liu, S. Li, M. Zeleke, Q. Liu, Z. Wang, A non-ordinary state-based peridynamics modeling of fractures in quasi-brittle materials, International Journal of Impact Engineering 111 (2018) 130-146.

[62] M. Liu, Q. Wang, W. Lu, Peridynamic simulation of brittle-ice crushed by a vertical structure, International Journal of Naval Architecture and Ocean Engineering 9 (2) (2017) 209-218.

[63] T. Rabczuk, H. Ren, A peridynamics formulation for quasi-static fracture and contact in rock, Engineering Geology 225 (20) (2017) 42-48.

[64] M. Behzadinasab, T.J. Vogler, A.M. Peterson, R. Rahman, J.T. Foster, Peridynamics modeling of a shock wave perturbation decay experiment in granular materials with intra-granular fracture. Journal of Dynamic Behavior of Materials (2018) 1-14 DOI: 10.1007/s40870-018-0174-2.

[65] C.J. Lammi, T.J. Vogler, Mesoscale simulations of granular materials with peridynamics. In AIP Conference Proceedings 1426(1) (2012) 1467-1470.

[66] T.J. Vogler, J.P. Borg, D.E. Grady, On the scaling of steady structured waves in heterogeneous materials. Journal of Applied Physics 112(12) (2012) 123507.

Accepted Manuscript

[67] E.G. Gilbert, D.W. Johnson, S.S. Keerthi, A fast procedure for computing the distance between complex objects in three-dimensional space, IEEE Journal on Robotics and Automation 4 (2) (1988) 193–203.

[68] G. van den Bergen, Collisions Detection in Interactive 3D Environments, D. Eberly, Ed. Morgan Kaufmann Publishers, 2003.

[69] J. Baumgarte, Stabilization of constraints and integrals of motion in dynamical systems, Computer Methods in Applied Mechanics and Engineering 1 (1) (1972) 1–16.

[70] M.J. Panik, Linear Programming: Mathematics, Theory and Algorithms, Springer US, Boston, MA, 1996.

[71] C.L. Byrne, Applied Iterative Methods. A K Peters, Ltd., Wellesley, MA, USA, 2008.

[72] R.C. Hurley, J. Lind, D.C. Pagan, M.C. Akin, E.B. Herbold, In situ grain fracture mechanics during uniaxial compaction of granular solids, Journal of the Mechanics and Physics of Solids 112 (2018) 273-290.

[73] A.R. Russell, D.M. Wood, Point load tests and strength measurements for brittle spheres, International Journal of Rock Mechanics & Mining Sciences 46 (2) (2009) 272-280.

[74] H. Edelsbrunner, E.P. Mucke, Three-dimensional alpha shapes, ACM Trans. Graph. 13 (1) (1994) 43–72.

[75] The CGAL Project. CGAL User and Reference Manual, CGAL Editorial Board, 4.11 Edition, 2017.

[76] X. Xu, K. Harada, Automatic surface reconstruction with alpha-shape method, The Visual Computer 19 (7-8) (2003) 431-443.

[77] G.R. McDowell, A. Amon, The application of Weibull statistics to the fracture of soil particles. Soils and Foundations 40 (5) (2000) 133–141.

[78] Y. Nakata, A.F.L. Hyde, M. Hyodo, H. Murata, A probabilistic approach to sand particle crushing in the triaxial test, Géotechnique 49 (5) (1999) 567-583.

[79] Y. Nakata, Y. Kato, M. Hyodo, A.F.L. Hyde, H. Murata, One-dimensional compression behavior of uniformly graded sand related to single particle crushing strength, Soil and Foundations 41 (2) (2001) 39-51.

[80] K.J. Hanley, C. O'Sullivan, X. Huang, Particle-scale mechanics of sand crushing in compression and shearing using DEM, Soils and Foundations 55 (5) (2015) 1100–1112.

[81] K.T. Chau, X.X. Wei, Spherically isotropic, elastic spheres subject to diametral point load strength test. International Journal of Solids and Structures 36 (29) (1999) 4473-4496.

[82] W. Weibull, A statistical distribution function of wide applicability. J. Appl. Mech. 18 (1951) 293-297.

[83] G.R. McDowell, A physical justification for log e–log σ based on fractal crushing and particle kinematics, Géotechnique 55 (9) (2005) 697–698.

[84] B.B. Mandelbrot, The Fractal Geometry of Nature, W. H. Freeman and Company, New York, 1982.

Accepted Manuscript

[85] J. Fonseca, C. O'Sullivan, M.R. Coop, P.D. Lee, Non-invasive characterization of particle morphology of natural sands, Soils and Foundations 52 (4) (2012) 712–722.

[86] B. Zhao, J. Wang, 3D quantitative shape analysis on form, roundness, and compactness with μCT, Powder Technology 291 (2016) 262-275.

[87] T. Zingg, Beitrag zur schotteranalyse, Schweiz. Mineral. Petrogr. Mitt. 15, p. 52–56, 1935.

[88] Z. Gao, J. Zhao, Y. Yao, A generalized anisotropic failure criterion for geomaterials, International Journal of Solids and Structures 47 (22-23) (2010) 3166-3185.

[89] Z. Gao, J. Zhao, Evaluation on failure of fiber-reinforced sand, Journal of Engineering Mechanics 139 (1) (2013) 95-106.

[90] N. Guo, J. Zhao, The signature of shear-induced anisotropy in granular media, Computers and Geotechnics 47 (2013) 1-15.

[91] J. Zhao, N. Guo, Rotational resistance and shear-induced anisotropy in granular media, Acta Mechanica Solida Sinica 27 (1) (2014) 1-14.

[92] J. Zhao, N. Guo, Unique critical state characteristics in granular media considering fabric anisotropy, Géotechnique 27 (1) (2014) 1-14.

[93] Z. Gao, J. Zhao, Constitutive modeling of artificially cemented sand by considering fabric anisotropy, Computers and Geotechnics 41 (2012) 57-69.

[94] Z. Gao, J. Zhao, Strain localization and fabric evolution in sand, International Journal of Solids and Structures 50 (22-23) (2013) 3634-3648.

[95] Z. Gao, J. Zhao, A non-coaxial critical-state model for sand accounting for fabric anisotropy and fabric evolution, International Journal of Solids and Structures 106 (2017) 200-212.

[96] N. Guo, J. Zhao, A coupled FEM/DEM approach for hierarchical multiscale modelling of granular media, International Journal for Numerical Methods in Engineering 99 (11) (2014) 789-818.

[97] N. Guo, J. Zhao, Parallel hierarchical multiscale modelling of hydro-mechanical problems for saturated granular soils, Computer Methods in Applied Mechanics and Engineering 305 (2016) 37-61.

[98] N. Guo, J. Zhao, Multiscale insights into classic geomechanics problems, International Journal For Numerical and Analytical Methods in Geomechanics 40 (3) (2016) 367-390.

[99] N. Guo, J. Zhao, 3D multiscale modeling of strain localization in granular media, Computers and Geotechnics 80 (2016) 360-372.

Accepted Manuscript